A reexamination of the role of wave–wave interactions in ocean noise generation

A. C. Kibblewhite and C. Y. Wu[a]
Department of Physics, University of Auckland, Private Bag, Auckland, New Zealand

(Received 30 June 1987; accepted for publication 30 November 1988)

A close connection between microseisms and ocean-wave activity has been recognized for many years. Various mechanisms have been proposed to explain the interaction, most favored being nonlinear interactions between ocean surface waves. Interest in these processes has increased in recent years as underwater acousticians have extended their investigations to infrasonic frequencies. This contribution builds on a study recently reported that confirmed the role of nonlinear wave–wave interactions at infrasonic frequencies but left some questions unresolved.

PACS numbers: 43.30.Ma, 43.30.Nb

INTRODUCTION

A recent article reported a study that examined the correlation of the ocean-wave field with wave-induced infrasonic pressure and seismic activity. The quality of the data, the long-term nature of the observations, and a unique property of the recording environment, helped establish that the acoustic-pressure field in the ocean below 5 Hz is controlled by nonlinear wave–wave interactions within the surface wave field. However, certain characteristics of the noise spectra remained unexplained.

It was apparent that these unexplained features were related, at least in part, to the angular distribution of the energy in the ocean-wave field and the geoacoustic properties of the ocean/seabed system. A preliminary analysis of these two effects was reported subsequently[2] but the precise nature of the influences involved still remained. As a first step towards assessing the influence of the seabed, a theoretical study based on a simple two-layer model was undertaken.[3] The present analysis examines the experimental evidence in the light of this study and expands upon a preliminary account.[4] While the limitations of the model are recognized, it does help provide some additional clarification of the processes involved.

I. BASIC THEORETICAL PREDICTIONS

As first reported by Miche,[5] consideration of second-order effects in the hydrodynamic equations leads to terms representing the generation of low-frequency pressure fluctuations by the nonlinear interaction of opposing ocean waves. In contrast to the progressive waves producing them, the distinctive features of these second-order effects are that the pressure signals they produce occur at twice the frequency of the interacting surface waves, are proportional to the amplitude product of these waves, and do not decrease with depth. Miche's theory was developed by Longuet-Higgins[6] to account for microseism generation and expanded further by Hasselmann[7] in particular. Similar theoretical analyses in the context of underwater acoustics were carried out by Brekhovskikh[8] and Hughes.[9] When minor errors are corrected,[10] the derived pressure spectrum can be shown to be essentially the same in all treatments.

While dealing with the same geophysical phenomenon, the various theoretical treatments are not easily reconcilable. For the purpose of the present analysis, therefore, it has been helpful to reexamine the theoretical basis of the phenomena involved, with a view to more readily resolving the significance of various factors, in particular, the effects of the spreading function associated with the surface-wave field and the properties of the geoacoustic environment.

This analysis, which we consider more clearly identifies the principal effects of concern, is presented elsewhere,[3] and only the results essential to the discussion that follows are presented here. These formulas show how the spectral forms of the low-frequency underwater pressure field and the associated seabed displacement are related to that of the surface-wave field in which the nonlinear interactions take place.

A simple geoacoustic model is assumed consisting of a water layer of constant depth H overlying an elastic half-space. The analysis demonstrates that the spectrum of the source pressure field, induced by wave action and acting on the mean surface of the ocean, is given by [see Eq. (50) of our companion article[3]]

$$F_P(f) = F_P(2f_W) = (32\pi^4\rho_1^2 g^2/\alpha_1{}^2)F_a^2(f_W)f_W{}^3 I$$

or (1)

$$F_P(f) = (4\pi^4\rho_1^2 g^2/\alpha_1{}^2)F_a^2(f/2)f^3 I.$$

{Here, we define the source pressure field as the homogeneous component of the total acoustic wave field induced by the second-order wave–wave interaction, which can be measured in an infinitely deep ocean. These components correspond to plane acoustic waves with horizontal wavenumber $k \ll \omega/\alpha_1$. The effects of the inhomogeneous component ($k > \omega/\alpha_1$) can be taken into account by introducing a mul-

[a] On leave from the Shanghai Acoustics Laboratory, Academia Sinica, Shanghai, People's Republic of China.

tiplying factor $[1+\eta_{ir}(\omega,z)]$ to the corresponding spectral expressions. This is explained in the companion article.[3]} The spectrum of the corresponding underwater noise field $F_N(f)$ and that of the microseisms (the displacement of the seabed) $F_M(f)$, are then given, respectively, by

$$F_N(f)=F_P(f)T_{PN}(f) \tag{2}$$

and

$$F_M(f)=F_P(f)T_{PM}(f), \tag{3}$$

where

$$T_{PN}(f)=2\int_0^1 \frac{|J(\kappa^2,\omega^2,z)|^2}{|J(\kappa^2,\omega^2|^2}\kappa\, d\kappa, \tag{4}$$

$$T_{PM}(f)=\frac{2}{\rho_1^2\omega^2\alpha_1^2}\int_0^1 \frac{1-\kappa^2}{|J(\kappa^2,\omega^2)|^2}\kappa\, d\kappa. \tag{5}$$

In the above equations, $f_W\equiv f/2$ denotes the frequency of the ocean surface wave; f is the frequency of the wave-induced source pressure field and its seismic equivalent; $\omega=2\pi f$; ρ_1 is the density of seawater, and α_1 the sound velocity in water; $F_a(f_W)$ is the surface-wave spectral function; $T_{PN}(f)$ and $T_{PM}(f)$ are the transfer functions relating the source pressure field on the sea surface to the underwater noise and seismic fields, respectively. The function $J(\kappa^2,\omega^2,z)$ is defined as

$$\begin{aligned}J(\kappa^2,\omega^2,z)&=\sin\left(\frac{\omega}{\alpha_1}\sqrt{1-\kappa^2}(z+H)\right)\\&\quad+i\frac{m}{n_\beta{}^4}\frac{\sqrt{1-\kappa^2}}{\sqrt{n^2-\kappa^2}}[(2\kappa^2-n_\beta^2)^2\\&\quad+4\kappa^2\sqrt{n^2-\kappa^2}\sqrt{n_\beta^2-\kappa^2}]\\&\quad\times\cos\left(\frac{\omega}{\alpha_1}\sqrt{1-\kappa^2}(z+H)\right),\end{aligned} \tag{6}$$

or, more generally,

$$\begin{aligned}J(\kappa^2,\omega^2,z)&=\sin\left(\frac{\omega}{\alpha_1}\sqrt{1-\kappa^2}(z+H)\right)\\&\quad+i\left(\frac{1+R_b}{1-R_b}\right)\cos\left(\frac{\omega}{\alpha_1}\sqrt{1-\kappa^2}(z+H)\right),\end{aligned}$$

where

$$J(\kappa^2,\omega^2)=J(\kappa^2,\omega^2,0).$$

In all of the above equations, we use: the parameters $n_\beta=\alpha_1/\beta_2$, $n=\alpha_1/\alpha_2$, $m=\rho_2/\rho_1$, $\kappa=k\alpha_1/\omega$; R_b the seabed reflection coefficient; and ρ_2, β_2, α_2, which are, respectively, the density and the wave velocities of the shear and compressional waves in the seabed.

The term I in Eq. (1) represents an integral of the spreading function describing the angular distribution of the surface-wave field,[7,11] viz.,

$$I\equiv\int_{-\pi}^{\pi}H(\theta)H(\theta+\pi)d\theta, \tag{7}$$

where $H(\theta)$ is the normalized spreading function defined as

$$H(\theta)=\frac{1}{H_0}G(\theta),\quad H_0=\int_{-\pi}^{\pi}G(\theta)d\theta. \tag{8}$$

From Eqs. (4) and (6) it is apparent that the underwater noise field is generally depth dependent. When z approaches zero, the transfer function $T_{PN}(f)$ tends to 1, which is simply a confirmation of the continuity of the pressure field.

II. THE OCEAN-WAVE SPECTRA

Most of the data discussed in this article were recorded in the South Taranaki Bight (the Maui region) on the west coast of the North Island of New Zealand (Fig. 1). In this region, the wave field is essentially fetch-limited at the Maui recording site for winds from the southeasterly quarter.[12] Discounting the influence of a persistent swell from the southwest (which will be considered further later), the JONSWAP formula[13]

$$F_a(f_W)=\alpha g^2(2\pi)^{-4}f_W{}^{-5}\exp[-\tfrac{5}{4}(f_W/f_M)^{-4}]\times\gamma^{\exp[-(f_W/f_M-1)^2/(2\sigma^2)]} \tag{9}$$

has been shown to fit the measured fetch-limited spectra very well, the average parameters for this MAUI spectrum being[12,14]

$$\alpha=0.07(U_{10}^2/gX)^{0.27}, \tag{10}$$

$$f_M=2.59(g^{0.72}/U_{10}^{0.44}X^{0.28}), \tag{11}$$

$$\gamma=2.9, \tag{12}$$

$$\sigma=\begin{cases}0.10, & \text{for } f_W\leqslant f_M,\\ 0.13, & \text{for } f_W>f_M,\end{cases} \tag{13}$$

in which X denotes the length of the southeasterly fetch in meters and U_{10} the wind speed at a height of 10 m. The derived spectra for $U_{10}=2.5$ to $30\,\mathrm{m\,s^{-1}}$ are shown in Fig. 2. (The reason for the units used will become clear later.)

III. THE INFLUENCE OF THE SPREADING COEFFICIENT ON THE PRESSURE FIELD

From Eqs. (7) and (8), we see that the term I is given by

$$I=\frac{1}{H_0^2}\int_{-\pi}^{\pi}G(\theta)G(\theta+\pi)d\theta. \tag{14}$$

In the case of a single sea (i.e., a sea generated by a steady wind, from a fixed direction, across an initially quiescent surface) a widely accepted form of the spreading function $G(\theta)$ is that proposed by Longuet-Higgins and recently compared with measured data by Tyler *et al.*,[11] viz.,

$$G(\theta)=\cos^{2s}(\theta/2),\quad -\pi\leqslant\theta\leqslant\pi, \tag{15}$$

with a spreading coefficient s, which usually appears to be both frequency and wind speed dependent.

By substituting Eq. (15) into (14), we obtain an analytical form of I[14]:

$$I(s)=(1/2^{(2s+1)}\sqrt{\pi})[\Gamma(s+1)/\Gamma(s+\tfrac{1}{2})], \tag{16}$$

in which $\Gamma(u)$ is the gamma function.

In the case of an omnidirectional wave field, it follows that

$$s=0 \text{ and } I(0)=1/2\pi, \tag{17}$$

while as

$$s\to\infty,\quad I(s)\to 0. \tag{18}$$

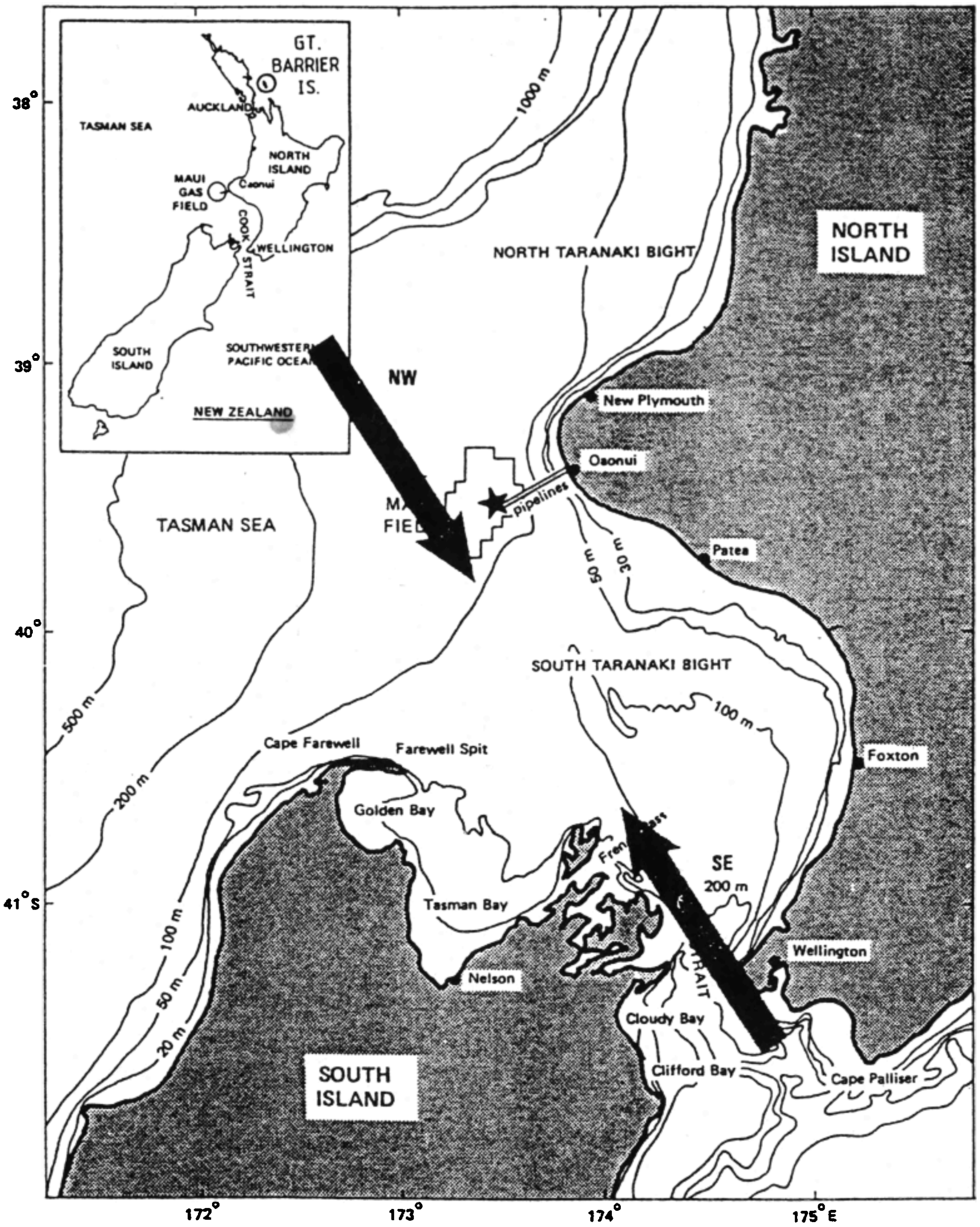

FIG. 1. Localities and bathymetry of Cook Strait and the Maui environment. The waverider buoy is installed close to the Maui platform and the receiving insrumentation and the seismometer ashore at Oaonui.

Stewart and Barnum[15] found the following form of s to fit Tyler *et al.*'s measured data very well[14]:

$$s\begin{cases}\approx 0.2/(\mu-0.1), & \mu\geqslant 0.1,\\ =2, & \mu<0.1.\end{cases} \tag{19}$$

The parameter μ is defined as

$$\mu=u_*/kc, \tag{20}$$

where $k=0.4$ (the Karman's constant), c is the speed of the surface wave and u_* the friction velocity.[1]

Using the values $u_*=U_{10}\sqrt{c_{10}}$, $c_{10}=1.5\times10^{-3}$, and noting that $c=g/(2\pi f)$ for gravity waves, we have

$$\mu\approx 0.062U_{10}f, \tag{21}$$

whereupon

$$s(f,U_{10})\begin{cases}\approx 2/(f/f_0-1), & f>f_0,\\ =2, & f<f_0,\end{cases} \tag{22}$$

with

$$f_0=\frac{1}{0.62U_{10}}\approx\frac{1}{6.08}\frac{g}{U_{10}}. \tag{23}$$

This model of s is shown in Fig. 3 by the dashed line from A to B to C (infinity) and then along the curve to D. The infinite discontinuity of the function s at point $f/f_0=1$ and a small constant value $s=2$ in the region $f/f_0<1$ suggests that the angular distribution of the wave energy becomes a δ function (very narrow beam) at the "resonant" frequency for the given wind speed U_{10}, and becomes wider at lower values of $f(f<f_0)$, even though, physically, this seems to be somewhat puzzling.

Other forms of the function s have been used, such as in Ref. 16:

$$s=\begin{cases}0.2/(\mu-0.1), & \mu\geqslant 0.2,\\ 2, & \mu<0.2,\end{cases} \tag{24}$$

where

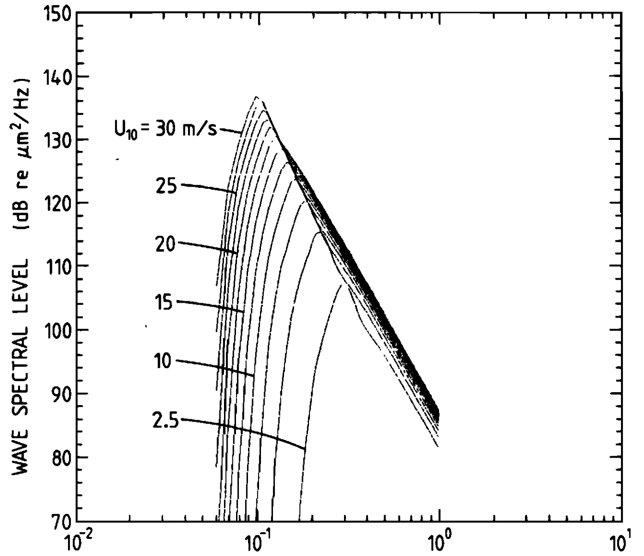

FIG. 2. Fetch-limited ocean-wave spectra derived using the JONSWAP formula with the Maui parameters, for wind speeds from 2.5 to 30 m s^{-1} at intervals of 2.5 m s^{-1}.

$$\mu = \begin{cases} 3.65\times 10^{-6} U^{5/4}\sqrt{f_0}, & U \leqslant 15 \text{ m s}^{-1}, \\ 8.33\times 10^{-6} U\sqrt{f_0}, & U > 15 \text{ m s}^{-1}, \end{cases}$$

and f_0 is the radar frequency ($f_0 = 30\times 10^6$ Hz). However, for ease of comparison with experimental data, we have introduced an adjustable parameter δ and write (it also seems appropriate to take $f_0 = f_r = g/(2\pi U_{10})$ instead of $g/6.02U_{10}$)

$$s = \begin{cases} 2/(f/f_0 - 1), & f \geqslant f_0(1+\delta), \\ 2/\delta, & f < f_0(1+\delta). \end{cases} \qquad (25)$$

Curves of s (as a function of f/f_0) for different values of δ are shown in Fig. 3. For a chosen δ (e.g., $\delta = 1.0$), s is described by the horizontal line (ABE) and the curve (ED). With δ specified, the integral I defined by Eq. (14) can easily be calculated. The form of I so obtained is shown in Fig. 4.

Since the spectrum of the source pressure field $F_P(f)$ is (apart from a constant) given by the product of the integral I, the square of the wave spectrum $F_a^2(f/2)$, and the term

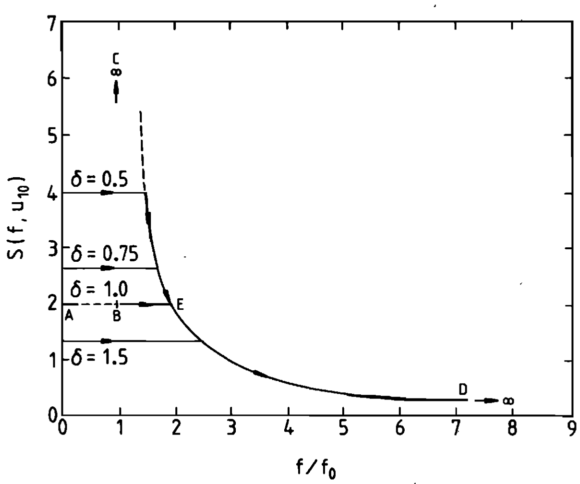

FIG. 3. The dependence of the spreading coefficient on δ.

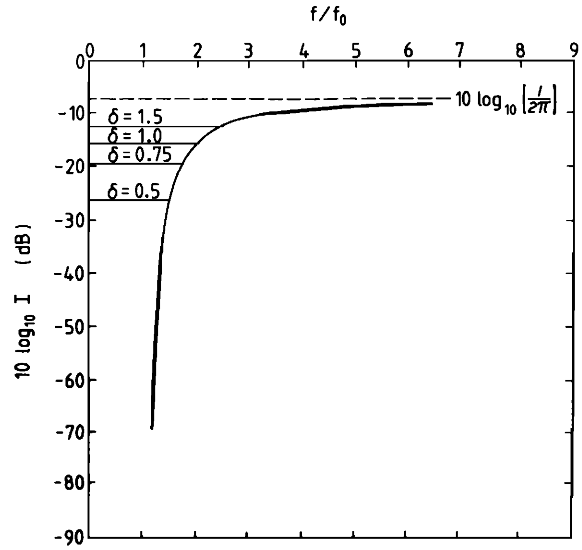

FIG. 4. The dependence of the integral I on δ.

f^3, the choice of δ will significantly change the value and position of the peak of the resulting spectrum $F_P(f)$. An estimate of the spreading coefficient can thus be obtained by matching the peak values of the measured and theoretical spectra of the pressure fields.

Figure 5 presents the calculated values of the peak of the pressure field spectra as a function of U_{10} for $\delta = 1.0$, 0.75,

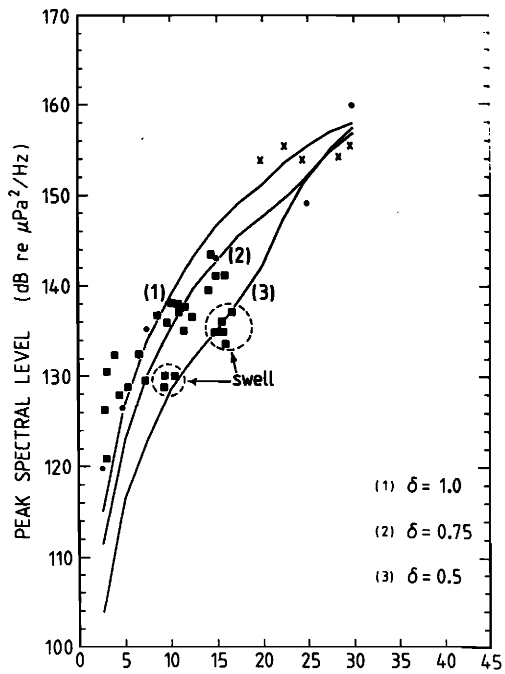

FIG. 5. A comparison of the peak levels of the wave-induced pressure field (full lines) derived from the Maui version of the JONSWAP function (for three values of δ), with experimental values of the ambient noise field derived from microseism spectra relevant to the same wind speed. The dots represent west coast data from the October 1981 events involving interactions within a single sea; the crosses represent data from the same events involving two interacting seas; the squares represent east coast data involving a single sea only.

and 0.5. In this figure, the dots and crosses represent experimental values determined from seismic spectra (see later) measured at different times, but mainly during a period in October 1981. The experimental values for wind speeds greater than 30 m s^{-1} were sampled soon after a wind change and reflect the interaction of two seas, see Sec. V. The other data were sampled at times when a single sea would be dominant. (The circled data points, which appear anomalous, involved a single narrow spectrum peaked at $f < 0.1$ Hz and accordingly correspond to a swell rather than a local sea situation.) It would appear that for low wind speeds (less than 10 m/s) a reasonable value of δ is 1.0, while for high wind speeds the value of 0.75 is more appropriate. The decrease in the value of δ at high wind speeds (low resonant frequencies) can be attributed to the influence of a multilayered geoacoustic structure, as will be shown in a later article.

Except where specifically mentioned otherwise, for simplicity we will take $\delta = 1$ as a reasonable approximation in the calculations to follow. Thus we define the spreading coefficient s as

$$s = \begin{cases} 2/(f/f_0 - 1), & f > 2f_0, \\ 2, & f \leqslant 2f_0. \end{cases} \tag{26}$$

By using Eqs. (9), (26), and those involving the calculation of the integral I, we can than derive the set of theoretical spectra for the source pressure field shown in Fig. 6.

IV. THE TRANSFER FUNCTION

The seabed displacement data discussed in this article were measured at an onshore station about 1 km from the coastline. Since the observation point is located so close to the active ocean region (in this case, within a distance of the order of 0.1 wavelength), Kibblewhite and Ewans[1] considered it reasonable to assume that the microseism activity recorded would not differ significantly from that existing within the active region. Accordingly, a simple two-layer fluid model was assumed and the ground vibration was attributed solely to the vertical displacement produced by the compressional wave, and the simplest transfer function[17] was applied to calculate the incident pressure field from the seismic spectra, a procedure that neglected any bottom reflections. In this reevaluation of the underwater noise field, based on the two-layered viscoelastic model discussed in Ref. 3, we examine the implication of bottom reflection and the generation of shearwaves. As explained in Ref. 3, the transfer functions used refer only to the homogeneous component of the pressure field.

When only compressional waves are being considered, we can put $\beta_2 = 0$ or $n_\beta = \infty$ in Eq. (6). Moreover, since in our present case the water-layer depth is not great, it is appropriate to use the approximations in Eq. (6) that

$$\sin[(\omega/\alpha_1)\sqrt{1-\kappa^2}(z+H)] = 0$$

and

$$\cos[(\omega/\alpha_1)\sqrt{1-\kappa^2}(z+H)] = 1.$$

This leads to the approximate transfer function;

$$T_{NM} \approx T_{PM} \approx a/\rho_1^2\omega^2\alpha_1^2, \tag{27}$$

with

$$a = (1 - 2n^2 + 2n^4)/2m^2. \tag{28}$$

The transfer function for four forms of this simple geoacoustic model, typical of the New Zealand environment, has been calculated by a numerical integration procedure. The results obtained, together with that for the simplest formula [case 5, $T_{PM} = 1/(\rho_1^2\omega^2\alpha_1^2)$] are shown in Fig. 7. The parameters used and the value of the coefficient based on Eq. (28), are listed in Table I.

From Fig. 7 and Table I it can be seen that over the frequency range of interest in this analysis (0.1–1.0 Hz), Eq. (27) adequately describes the frequency dependence of the transfer function, the difference from the curves based on the full expression being less than 1 dB. The frequency dependence of Eq. (27) is thus confirmed as a good approximation

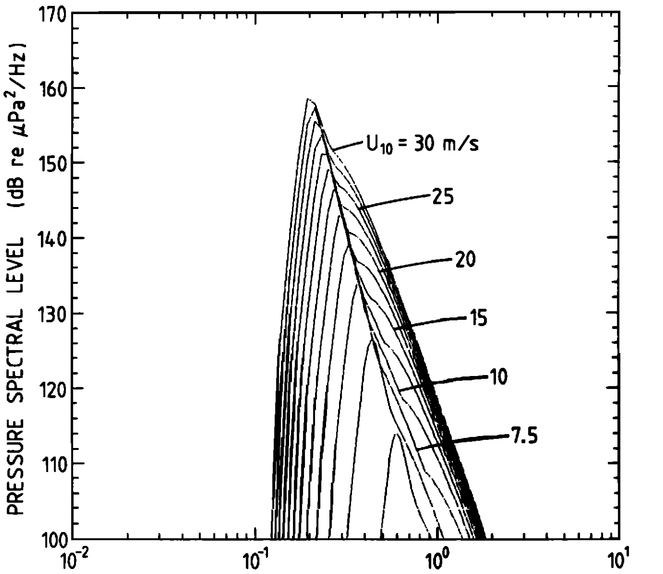

FIG. 6. Spectra of the theoretical pressure field for wind speeds from 2.5–30 m s^{-1}.

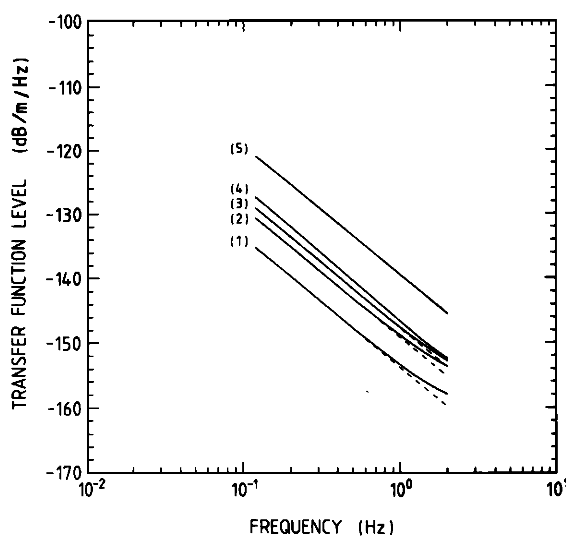

FIG. 7. The complete (curves) and approximate (straight lines) compressional-wave transfer functions for different geoacoustic models.

TABLE I. The dependence of the coefficient a on the model type.

Model	m	n	a	$10 \log_{10} a$	Ref.
1	2.7	0.83	0.0392	− 14.07	20
2	2.0	0.9615	0.1076	− 9.69	19
3	1.29	0.78	0.16	− 8.03	–
4	1.04	0.64	0.24	− 6.22	–
5			Urick		17

and its application with $a = 1$ in Ref. 1 is shown to be reasonable.

It should be noted, however, that T_{PM} is the transfer function that converts the spectrum of the source pressure field at the sea surface to that of the vertical displacement of the seabed, and that $T_{MP} = (T_{MP})^{-1}$ should be used for the inverse transfer function. In this case, $T_{MP}(=\rho_1^2\omega^2\alpha_1^2/a)$ is generally greater than $\rho_1^2\omega^2\alpha_1^2$ for models with $m>1$. Urick[17] drew attention to this, although the influence of reflection at the seabed was neglected in his analysis. It is apparent from Fig. 7 that the influence of a on the magnitude of T_{MP} cannot be ignored. This was recognized by Urick and also by Kibblewhite and Ewans[1] (Sec. V A) but at that time the precise influence of a could not be established. It is now appropriate to reconsider this issue, and, in the next part of our analysis, we review the event of October 1981.

V. THE EVENT OF 16–24 OCTOBER 1981

The Maui region provides an ideal environment for the study of ocean-wave processes in that the topography of Cook Strait often produces a bimodal wind regime in the area as weather systems pass across the country. These properties are described in the earlier article[1] that presented the meteorological events of October 1981 to describe the effects observed. The time histories of the relevant parameters during these events are presented in Fig. 2. This shows clearly the wave and seismic response to the wind changes on 16 and 23 October, when the wind vector swings rapidly through 180° from northwest to southeast.

Figure 8, which is reproduced from Ref. 1, presents the series of spectra $F_P(f)$, describing the pressure field produced by nonlinear wave–wave interactions during the first of these southeasterly events. (Since, here, the depth of the water layer is only a small fraction of the wavelength concerned, we neglect the depth dependence of the noise field and regard both the ambient noise pressure and the source pressure fields as being the same.) These spectra were derived from the corresponding vertical displacement spectra $F_M(f)$ by applying the approximate form of the transfer function $1/[\rho_1^2\omega_1^2\alpha_1^2]$, where $\omega = 2\pi f$.

In Ref. 1, these experimental pressure spectra were compared with ocean ambient noise data recorded in other environments by conventional methods, and attention was drawn to the striking similarities that existed. The pressure spectra derived from the seismic measurements were also compared with theoretical predictions based on the nonlinear interaction formalisms of Brekhovskikh and Hughes.[8,9] The agreement between predicted and observed spectral levels was equally striking, particularly around the spectral peaks and for high sea states. Attention was also drawn to the apparently anomalous low-frequency component in the experimental spectra, which became obvious at low wind speeds, and to an inflexion (or subsidiary peak) around 0.5 Hz visible in the spectra for wind speeds of 7.5, 15, and 25 m s^{-1} (Fig. 8).

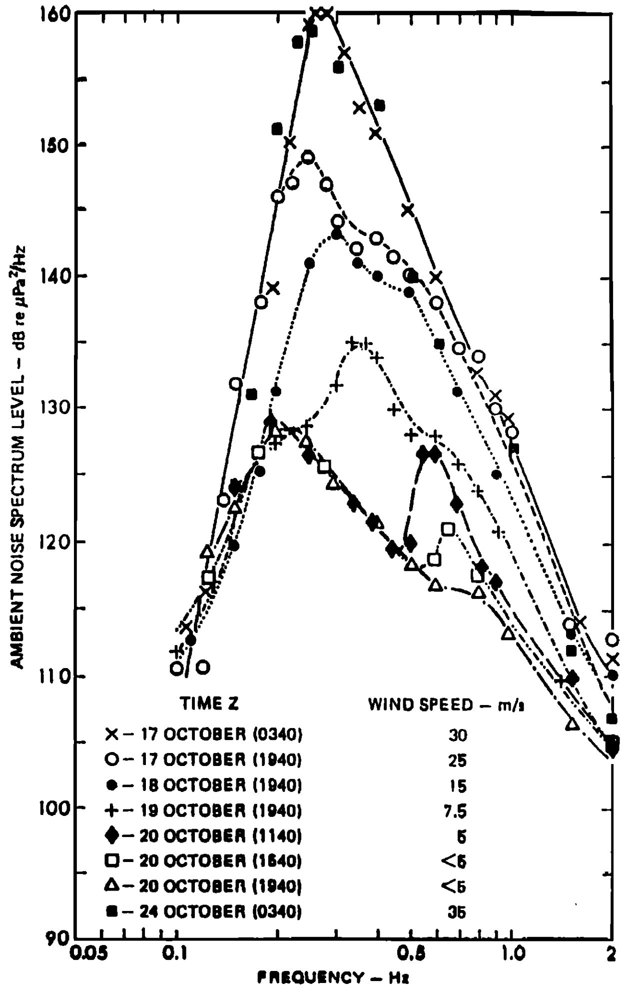

FIG. 8. Ambient noise levels derived from the seismic spectra as a function of wind speed—event 17 October 1981.

The first of these two effects was shown to arise from the persistent southwesterly swell that is always present in the recording area. Possible explanations were offered for the second feature but a definitive statement could not be given at that time because it was not possible to resolve clearly between the relative influence of the spreading and transfer functions. It is work on these questions that is the main subject of this and its companion article.[3]

Based on this latest analysis, the theoretical pressure spectra arising from nonlinear interactions within a single sea, when the assumed value $\delta = 1.0$ is used to evaluate the spreading function, are those given in Fig. 6. A comparison with those for the same wind speeds derived from the experimental seismic data is presented in Fig. 9.

It can be seen: (i) that the large low-frequency component apparent in the experimental data at low wind speeds is not present in the theoretical spectra; (ii) that a small but

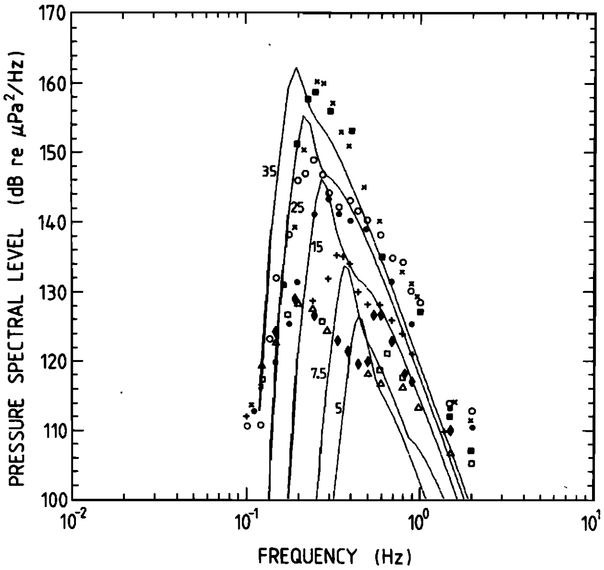

FIG. 9. Comparison of the theoretical pressure spectra for a single sea with those derived from the measured seismic data (Fig. 8), using the approximate transfer function $T_{MP} = \rho_1^2 \omega^2 \alpha_1^2$.

significant difference in the peak frequencies of the two sets of spectra is apparent at high wind speeds but that this difference decreases as the wind decreases; (iii)that both sets of spectra display a subsidiary peak (inflexion) around 0.5 Hz at wind speeds above 7.5 m s^{-1}; (iv) that while the peak spectral levels show good agreement, the levels at frequencies well above the peak are noticeably higher in the experimental spectra.

As mentioned earlier, the low-frequency peak described in (i) above is associated with the southwesterly swell, which is always present in the Maui region. This is clearly demonstrated in the spectra for various wind speeds presented in Fig. 10. (The JONSWAP form of the Maui spectra reproduced in Fig. 2 deliberately omitted these components in the interest of simplicity.)

In contrast to the explanation given in Ref. 1, the differences described in (ii) above are now reinterpreted as meaning that the high spectral levels recorded at the early stage of the event (0340 on 17 October; × in Fig. 8) involve not only nonlinear interactions between components of the new southeasterly sea, but also continuing interactions between the new sea and residual components of the old northwesterly sea. Further, the inflexion around 0.5 Hz in Fig. 8 is now identified with the spreading function (rather than the transfer function as was suggested in Refs. 1 and 2). However, as will be shown, the influence of a second sea can produce a similar and often more dominant effect.

VI. THE CASE OF MULTIPLE SEAS

The situation described above is obviously complex. Nevertheless, accepting these interpretations we can test their validity through Eq. (29) (see the Appendix), which is an expression for the spectrum of the source pressure field resulting from the combined nonlinear interactions of the southwesterly swell, the decaying northwesterly sea, and the new sea from the southeast. Equation (29) is

$$F_P(f) = K_0 f_W^3 \left(\sum_{i=1}^{3} [F_a^i(f_W)]^2 I_{ii} + \sum_{i,j=1}^{3} F_a^i(f_W) F_a^j(f_W) I_{ij} \right), \tag{29}$$

where

$$K_0 = 32\pi^4 \rho_1^2 g^2 / \alpha_1^2, \tag{30}$$

$$f_W = \tfrac{1}{2} f, \tag{31}$$

$$I_{ii} = \Gamma(s_i + 1)/\sqrt{\pi}\, 2^{(2S_i+1)} \Gamma(s_i + \tfrac{1}{2}), \tag{32}$$

$$I_{ij} = \frac{1}{H_i H_j} \int_{-\pi}^{\pi} \left(\cos^2 \frac{\theta}{2}\right)^{S_i} \left[\sin^2\left(\frac{\theta}{2} + \frac{\theta_{ij}}{2}\right)\right]^{s_j} d\theta, \tag{33}$$

$$H_i = 2\sqrt{\pi}\,\Gamma(s_i + \tfrac{1}{2})/\Gamma(s_i + 1), \tag{34}$$

where $F_a^{i,j}(f_W)$ are the wave spectra of sea i and sea j.

In deriving this formula, we have assumed that the directivity of the southwesterly swell can also be expresed using a model based on a $\cos^2(\theta/2)$ distribution. This assumption is reasonable provided that the appropriate choice of the spreading coefficient s can be made. However, the actual

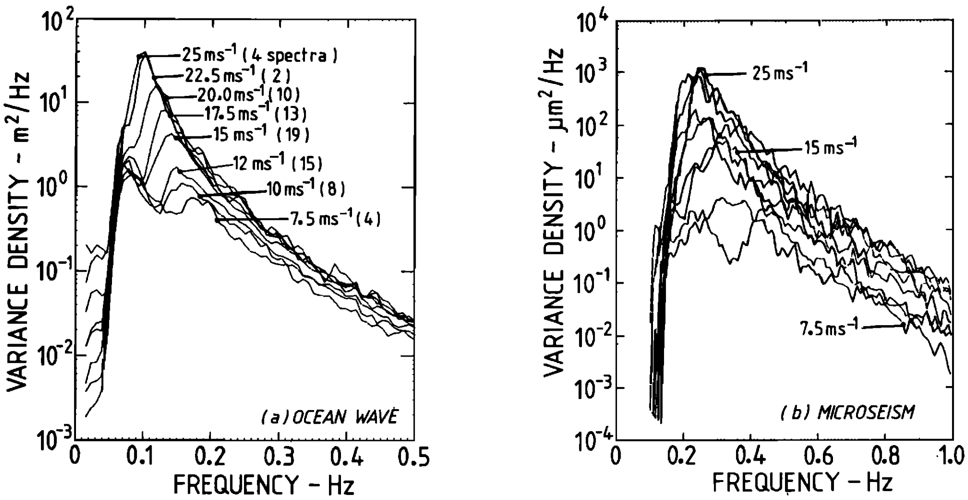

FIG. 10. Average ocean-wave and seismic spectra in the Maui region as a function of wind speed (reproduced with the permission of Reidel Pub. Co. from Ref. 4).

spectral forms of the energy associated with the residual swell from the southwest and the decaying sea from the northwest prove to be of more importance. Both of these are, of course, difficult to assess in the absence of directional wave data, but reasonable approximations can be made.

Our estimates of the decaying northwesterly sea are based on the JONSWAP expression and the selected wind speed. The uncertainties relating to the spectral form of the southwesterly swell have been addressed through the concept of the "average" spectrum for the area, developed for general statistical reasons in another study.[18] The average spectrum is defined as the average for given conditions of all the spectra recorded at the Maui site over a 2-year period (1980, 1981). Such a spectrum, based on seas associated with the southwesterly sectors (220°–230 °T) is shown in Fig. 11 [the dashed curve is the fitted form of the JONSWAP formula based on Eqs. (10) to (13), with the parameter $\gamma = 1$]. It demonstrates clearly the dominance of the southwesterly swell in the region, in spite of the high energy of the local wave-generation events. In this case, the peak value is about 2.5 m^2/Hz.

In applying Eq. (29), we assume a dominant southeasterly sea, a decaying northwesterly sea, and a residual southwesterly swell; for the latter, a value of 2 is used in respect of the spreading functions s_3. The calculation based on Fig. 11 led to the theoretical spectra shown in Fig. 12; the experimental spectra as originally derived from the seismic data (symbols) are included for comparison. Several features of these curves and those of Fig. 9 are to be noted.

(i) The experimental data for wind speeds 30 and 35 m s^{-1} appear to match the theoretical curve involving two separate seas (respective wind speeds 20, 15 m s^{-1}) better than that for a single sea excited by a wind speed of 30 to 35 m s^{-1}. While the peak spectral values in Fig. 9 are comparable, the theoretical spectrum for a single sea at high wind speeds, say 35 m s^{-1}, has a peak frequency around 0.2 Hz, lower than that of the measured data (0.25–0.3 Hz). In Fig. 12, on the

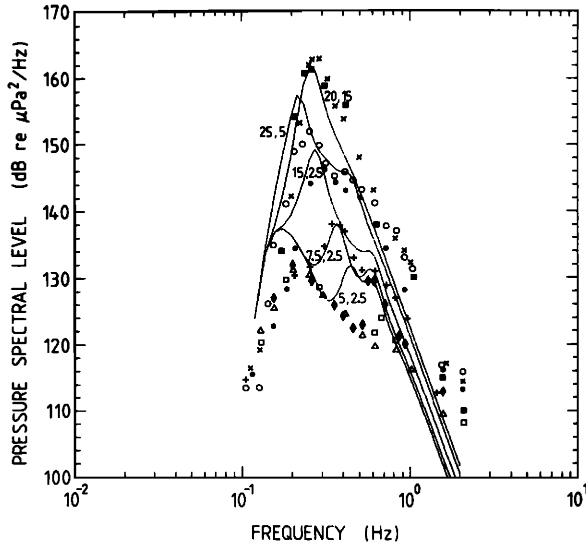

FIG. 12. A comparison of the theoretical pressure spectra resulting from nonlinear interactions of three seas with the experimental spectra derived from the seismic field using the transfer function $T_{MP} = \rho_1^2\omega^2\alpha_1^2/a$.

other hand, the frequencies of the spectral peaks at high wind speeds are much more in agreement.

(ii) While the experimental and theoretical spectral levels above the swell peak match reasonably well, the theoretical values at the swell peak suggest that the actual swell during the October event was somewhat lower than that represented by the average spectrum based on the southwesterly sectors.

(iii) At the top wind speeds in particular, the high-frequency spectral values are in general greater than those predicted theoretically.

At this point we recall that the transfer function used in deriving the experimental spectra (symbols in Fig. 8) from the corresponding seismic data is the approximate form used by Urick, $T_{MP} = 1/T_{PM} = \rho_1^2\omega^2\alpha_1^2$. It is, therefore, instructive to examine the effect of using the new transfer function given in Eq. (27), $T_{MP} = \rho_1^2\omega^2\alpha_1^2/a$.

Use of the new function increases all the seismically derived pressure values in Fig. 8 (and Fig. 12) by the value of 10 log a. For the models examined in Table I, the increase ranges from 6–14 dB depending on the model chosen. Overall, this adjustment appears to increase the anomalies, particularly at high wind speeds. Thus consideration of reflection losses alone does not further improve the agreement between theory and experiment and it becomes appropriate to examine the influence of shear-wave excitation and propagation effects.

According to the discussion in our companion article,[3] the transfer function takes the form $T_{MP} = \rho_1^2\omega^2\alpha_1^2/a[1 + \eta_T(\omega)]$ when shear-wave excitation is taken into account. Since $\eta_T(\omega) \approx A\omega$, use of the complete transfer function will involve an increase in the original spectral levels of only a few dB, considerably less than involved in — 10 log a alone. Such an adjustment would appear to bring the experimental data into closer overall agreement with the theoretical curves, but a test of this clearly depends on a detailed knowledge of the geoacoustic properties of the Maui region.

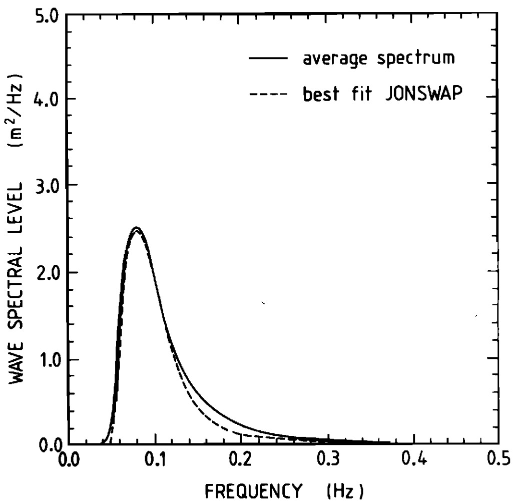

FIG. 11. The average wave spectrum at the Maui site (1980, 1981). The dashed curve corresponds to the Maui form of the JONSWAP formula with $\gamma = 1.0$.

VII. THE SEDIMENT-VELOCITY STRUCTURE

The basic transfer functions described in Fig. 7 refer to the idealized case of a water layer overlying a semi-infinite half-space. In model 1, the solid half-space represents a high-velocity basement layer; model 5 represents the case where $a = 1$, and no reflectivity or shear-wave excitation occurs. Models 2–4, on the other hand, represent other versions of the simple two-layer model and reflect, to varying degrees, the geophysical structure in the Cook Strait/Maui area.

From various published sources[19] and more recent geophysical data gathered as part of the oil/gas exploration program, the general characteristics of the area can be defined with reasonable confidence. In essence, the waters of the South Taranaki Bight overlay a layered seabed. The upper layer comprises unconsolidated sediments ($\rho_2 \approx 1700$ kg m^{-3}) of varying thickness but typically the lower interface (X) lies around a depth of 500 m in the vicinity of the Maui platform. The compressional wave velocity α_2 is about 1560 m s^{-1} so that $n = 0.9616$ can be adopted as representative. In turn, the unconsolidated sediment overlies further sedimentary layers. The nature and thickness of these varies somewhat with position but, in the area of interest to us, two further layers can be identified with compressional-wave velocities α_3 and α_4 of around 2000 and 3100 m s^{-1}, respectively. A thickness of approximately 750 m places the interface (Y) between layers 3 and 4 at approximately 1350 m. The horizon Q at the bottom of layer 4 is some 1675 m deeper. Typical densities are about 1900 and 2300 kg m^{-3}, respectively. Two deeper layers ($\rho_4 \approx 2500$ kg m^{-3}, $\alpha_4 \approx 3700$ m s^{-1}; $\rho_5 \approx 2500$ kg m^{-3}, $\alpha_5 \approx 4100$ m s^{-1}), occur before basement is encountered at around 3800 m.

With this information, but still restricting ourselves to a two-layer interpretation of the environment, we can examine the consequences of neglecting shear-wave effects in the earlier analysis. Where a shear-wave velocity for a layer is required, in Sec. VIII we have used the general expression $\beta = 0.58\,\alpha$.[20] This leads to a shear-wave velocity of around 1200 m s^{-1} for layer 3, a value of the same order as the Scholte-wave velocities for hard sediments quoted by Rauch.[21] We recognize, however, the constraints of the simple model used and that the velocity structure given is not likely to be uniform over the deeper parts of the active fetch. Where water depths exceed 1000 m, it is likely that interface X will disappear as the unconsolidated layer becomes much thinner.

VIII. THE SHEAR-WAVE CONTRIBUTION

In the analysis presented in Ref. 3, we established the modified transfer function for the simple two-layer model as

$$T_{MP} = \rho_1^2 \omega^2 \alpha_1^2 / a[1 + \eta_T(\omega)], \tag{35}$$

where

$$\eta_T(\omega) = 0.036\alpha_1^4 L_y \omega \eta(s_1,\omega)/\pi^2(1 - 2n^2 + 2n^4)\beta_2^5, \tag{36}$$

and L_y is the length and L_x the width of the active fetch, $\eta(s_1,\omega) \approx 1$ in the present case (see Ref. 3), β_2 is the shear-wave velocity in layer 2, and the other symbols have the meaning given earlier.

Equation (35) implies that with both bottom enhancement and shear-wave excitation present, the simple transfer function used in deriving the pressure curves of Fig. 8 should be modified by the factor $a[1 + \eta_T(\omega)]$ or $10 \log a[1 + \eta_T(\omega)]$ dB.

Equations (35) and (36) clearly represent the body and Rayleigh wave contributions from a homogeneous half-space. In the absence of the full multilayer analysis, they are now, in turn, applied to the three top interfaces in the sedimentary profile (the absence of significant structure in the seismic spectra below 1 Hz suggested that the deeper structure was not dominant). While this procedure ignores any interface interaction, it will hopefully provide some measure of the magnitude of the shear-wave correction. In the following discussion, we follow the normal nomenclature in defining the interface waves.[21] In evaluating Eq. (36) the active fetch L_y has been taken as 400 km.

A. The seabed interface

Because of high shear-wave attenuation, the wave energy transmitted at the water/seabed interface is usually negligible, the Scholte waves being guided by the most significant acoustic interface.[21] This appears to be confirmed in the present case. The full transfer function of Eq. (35) based on model 3 implies that the experimental values in Fig. 8 should be decreased by 20 and 30 dB over the range 0.1–1 Hz. In other words, the low acoustical contrast of this interface produces adjustments clearly out of line with the theoretical curves and we next consider interface X.

B. Interface *X*

Substitution of the appropriate geophysical parameters for interface X in Eqs. (35) and (36) suggests that the pressure spectral values in Fig. 8 should, in this case, be decreased by a factor ranging from -1.0 dB at $f = 0.1$ Hz to 10.5 dB at 2 Hz. Applying these corrections to the data of Fig. 8 gives the modified ambient-noise spectra of Fig. 13. It appears that allowing for the shear-wave contribution leads to little change in the derived pressure spectra around 0.1 Hz, but to significant changes at 1 Hz. The effects of bottom reflectivity seem to be more or less compensated at 0.1 Hz and overcompensated at higher frequencies.

C. Interface *Y*

Similar calculations for interface Y, the boundary between layers 3 and 4, produce changes in spectral level of the same order of magnitude as those of X.

IX. THE THEORETICAL AND REVISED EXPERIMENTAL CURVES

Bearing in mind the complexities involved, the overall agreement in the shape and magnitude of the experimental curves as originally presented in Ref. 1 (see Fig. 8) and the theoretical curves (see Fig. 9) were considered good. This agreement is improved when the interaction of multiple seas is considered (see Fig. 12). The use of the transfer function incorporating bottom reflectivity alone worsens the mismatch of high frequencies and high seastates, but allowance

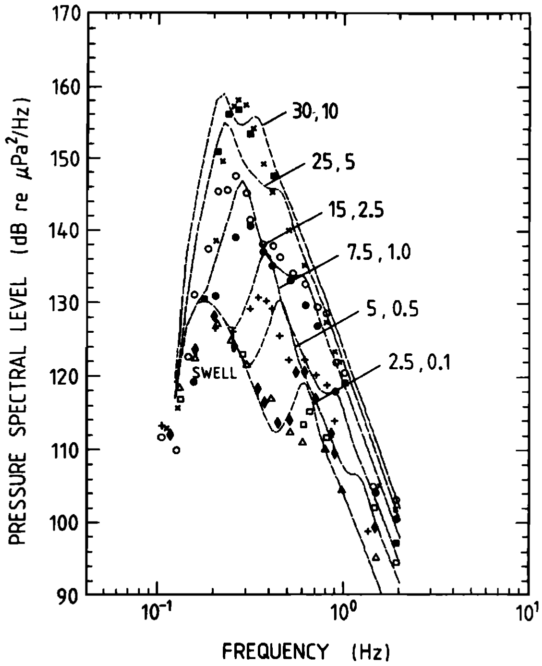

FIG. 13. A comparison of the theoretical pressure spectra resulting from nonlinear interactions of three seas with the experimental spectra derived from the seismic field using the transfer function appropriate to shear-wave activity ($\delta = 0.75$ for wind speeds greater than $10\ \mathrm{m\ s^{-1}}$).

for a shear-wave contribution based on interface X (or Y) through a modified version of the transfer function appears to produce a satisfying agreement in level and shape over the whole frequency range. The fact that a horizontal component of ground displacement was usually present,[14] that the theoretical and experimental levels at 1 Hz are both around 120 dB *re*: 1 μPa^2/Hz (a value reported for deep-sea ambient noise levels at moderate wind speeds[22]), and that the peak values agree closely, gives some confidence in the arguments presented.

Closer agreement still could be achieved by further minor changes in the three sea-wave components involved but this refinement is unjustified in the absence of directional wave data. Furthermore an unequivocal comparison of the theoretical and experimental curves must await the development of the full multilayer analysis discussed in Ref. 3. Schmidt *et al.*[23] have already demonstrated the influence of interface waves on source levels at frequencies below acoustic cutoff, and only when these effects are better understood, will further refinements be justified in the present case. It is, however, encouraging that the mismatch at high frequencies apparent in the comparison of Fig. 12 is now largely removed and that the theoretical and amended experimental results of Fig. 13 show remarkable agreement at all frequencies and for all wind speeds.

X. FREQUENCY DEPENDENCE OF THE NOISE FIELDS

Part of the analysis carried out by Kibblewhite and Ewans[1] was a comparison of the high-frequency spectral slopes of the ocean-wave and displacement spectra. (Secs. III C and V B). The results of this comparison were presented as evidence in support of the basic theoretical formulation relating microseisms and nonlinear wave–wave interactions. It is appropriate to review these earlier conclusions in the light of the theoretical analysis presented in our comparison article.[3]

In that analysis, it was shown that the connection between related spectra can be expressed through corresponding transfer functions as detailed in Eqs. (2) and (3) presented earlier. Further, when the depth of the water layer is much less than the wavelength of the components of the acoustic-noise field, the transfer fucntion $T_{PN}(\omega)$ was shown to be essentially independent of frequency. In the case of a near field sensor, it follows (inside the active region) that

$$F_P(\omega) \propto F_a^2(\omega/2)I(\omega)\omega^3, \tag{37}$$

$$T_{PM}(\omega) \propto \omega^{-2}, \quad \text{if } \beta_2 = 0, \tag{38}$$

$$\propto \omega^{-2} \int_0^1 \frac{1-\kappa^2}{|J(\kappa^2,\omega^2)|^2}\,\kappa\, d\kappa, \quad \text{if} \quad \beta_2 \neq 0. \tag{39}$$

We note that Eq. (38) is similar to the transfer function proposed by Urick[17] and used by Kibblewhite and Ewans[1] and that Eq. (39) is the same as Eq. (5).

In the farfield case, on the other hand, these expressions become

$$F_P(\omega) \propto F_a^2(\omega/2)I(\omega)\omega \tag{40}$$

and

$$T_{PM}(\omega) \propto \omega. \tag{41}$$

In Eq. (41), we recognize the function derived by Hasselmann.[7] [In fact, in the farfield case, the microseism activity is mainly contributed by Scholte wave components, so we can write $F_M(\omega) \sim \omega^2$ whereupon $F_M(\omega)/F_P(\omega) \sim \omega$.]

The experimental situation in Ref. 1 places the sensor intermediate between the near- and farfield regions. In view of this and the other complicating factors mentioned earlier, the observed frequency dependence of the microseism spectra might be expected to reflect a combination of the two effects described above.

In the earlier analysis[1] Hasselmann's transfer function was used [equivalent to Eq. (41)] to relate the general form of the microseism spectra to that of the wave field. In deriving the underwater pressure field from the displacement spectra on the other hand, use was made of Urick's form of the transfer function [equivalent to Eq. (38). The apparent inconsistency was recognized at the time but only justified later when a combined transfer function was shown to be appropriate.[3] This function, which is reproduced in Eq. (35), can also be written in the form

$$T_{MP} = T_{PM}^{-1} \approx \omega^2/(1 + A\omega). \tag{42}$$

Equation (42) is simply an expression of the combined effects of the nearfield (compressional wave) and farfield (shear-wave) contributions. The apparent effectiveness of Eq. (42) in reconciling the experimental results and theoretical predictions was demonstrated in Sec. IX.

The effect of the influences described in the present analysis on high-frequency spectral slopes can be summarized as follows.

(i) If an average ocean-wave spectrum is adopted

$[F_a^2(\omega) \propto \omega^{-9}$ to ω^{-10}—see Ref. 1, Sec. III C] the spectral slope of the underwater pressure field will, according to Eq. (37), be between ω^{-6} and ω^{-7}. The experimental pressure spectra derived from the seismic data for high wind speeds and steady conditions are in reasonable agreement with this theoretical prediction when the combined transfer function of Eq. (42) is used. It has been observed, however, that the seismic spectral slope (and that of the associated pressure field) can climb to ω^{-9} under the influence of a shift in wind direction and the growth of a new sea. As the wind steadies and the new sea exerts an increasing influence on the seismic spectrum the spectral slope decreases from ω^{-9} to ω^{-6} to ω^{-7}. This slope persists as the wind decreases. The change in slope is believed to arise from the fetch dependence of the growing sea.

(ii) The integral $I(\omega)$ depends strongly on the spreading coefficient of the wave energy distribution. In the event of a wind shift $I(\omega)$ will influence the value of the spectral peak and produce associated changes in spectral slope.

While both these factors will influence the spectral slope, the observed frequency relationship between the wave field and the noise fields can, as observed by Kibblewhite and Ewans,[1] still be taken as confirmation of the essential features of the theoretical formalism governing nonlinear interactions.

XI. CONCLUSIONS

The earlier analysis presented in Ref. 1 confirmed the role of wave–wave interactions in ocean acoustic phenomena at frequencies below 5 Hz. In that analysis, the essential elements of the theoretical background to nonlinear processes were confirmed. However, several aspects required further clarification, in particular, the role of multiple seas, and the relative influence of the spreading function and the transfer functions on the shape and magnitude of the related spectra.

In this and a companion article[3] it has been shown that while the transfer function used in Ref. 1 to relate the seismic field to the incident acoustic pressure was simplistic, the essential conclusions of that analysis were correct. However, the real properties of the spreading function and the various transfer functions are now more clearly understood and the interactions involved are seen as being more complex than previously believed. While an even closer agreement between theoretical predictions and the measured data has been established and the basic theoretical analyses have been confirmed, it is clear some matters still require clarification. In particular, we recognize the need for a more complete analysis of the effects of the multilayered seabed. The simple two-layer model has been instructive but is obviously an oversimplification. Until the multilayer analysis is complete, directional wave spectral data are available, and other influences including that of the inhomogeneous component are assessed more fully, the close quantitative agreement between theory and experiment implicit in these results cannot be accepted without reservation.

Through this study it has also been possible to obtain an independent assessment of the spreading function controlling the angular distribution of ocean-wave energy. This has involved a comparison of the theoretical predictions of the pressure field produced by nonlinear interactions between ocean-surface waves and the pressure field derived from the measured seismic field these interactions produce. A modified form of the spreading function is proposed on the basis of this comparison.

ACKNOWLEDGMENTS

This article develops ideas that first arose in the course of the Ph.D. studies pursued by Dr. K. C. Ewans. The major contribution made in that earlier work and its relevance to this and its companion article is warmly acknowledged.

APPENDIX: PRESSURE FIELD ARISING FROM NONLINEAR INTERACTIONS BETWEEN MULTIPLE SEAS

Equation (1) can be written as

$$F_P(f) = K_0 f_W^3 \int_{-\pi}^{\pi} F_a(f_W) H(\theta) F_a(f_W) H(\theta+\pi)\, d\theta, \tag{A1}$$

by denoting

$$K_0 = 32\pi^4 \rho_1^2 g^2/\alpha_1^2. \tag{A2}$$

In the case involving multiple independent seas, Eq. (1) can be extended as

$$\begin{aligned} F_P(f) &= K_0 f_W^3 \int_{-\pi}^{\pi} \sum_i F_a^i(f_W) H^i(\theta) \sum_j F_a^j(f_W) H^j(\theta+\pi) d\theta, \\ &= K_0 f_W^3 \left(\sum_{i=1}^{3} F_a^i(f_W) I_{ii} + \sum_{i,j=1(i\neq j)}^{3} F_a^i(f_W) F_a^j(f_W) I_{ij} \right), \end{aligned} \tag{A3}$$

where

$$I_{ii} = \int_{-\pi}^{\pi} H^i(\theta) H^i(\theta+\pi) d\theta = \frac{1}{H_i^2} \int_{-\pi}^{\pi} \cos^{2S_i}\left(\frac{\theta}{2}\right) \sin^{2S_i}\left(\frac{\theta}{2}\right) d\theta = \frac{\Gamma(s_i+1)}{\sqrt{\pi}\, 2^{(2S_i+1)} \Gamma(S_i+\frac{1}{2})} \tag{A4}$$

$$I_{ij} = \frac{1}{H_i H_j} \int_{-\pi}^{\pi} \left[\cos^2\left(\frac{\theta}{2}\right)\right]^{S_i} \left[\sin^2\left(\frac{\theta}{2} + \frac{\theta_{ij}}{2}\right)\right]^{S_j} d\theta, \tag{A5}$$

θ_{ij} is the crossing angle of sea i and sea j, and $F_a^i(f_W)$ and $F_a^i(f_W)$ are the wave spectra of sea i and sea j, respectively.

[1]A. C. Kibblewhite and K. C. Ewans, "Wave–wave Interactions, Microseisms, and Infrasonic Ambient Noise in the Ocean," J. Acoust. Soc. Am. **78**, 981–994 (1985).

[2]A. C. Kibblewhite and K. C. Ewans, "A Study of Ocean and Seismic Noise at Infrasonic Frequencies," in *Ocean-Seismo-Acoustics*, edited by T. Akal and J. M. Berkson, (Plenum, New York, 1986).

[3]A. C. Kibblewhite and C. Y. Wu, "The Generation of Infrasonic Ambient Noise in the Ocean by Nonlinear Interactions of Ocean Surface Waves," J. Acoust. Soc. Am. **85**, 1935–1945 (1989).

[4]A. C. Kibblewhite, "Ocean Noise Spectrum Below 10 Hz—Mechanisms and Measurements," in *Sea Surface Sound*, edited by B. Kerman (Reidel, Dordrecht, The Netherlands, 1988).

[5]M. Miche, "Mouvements Ondulatoires de la Mer en profondeur Constante ou Decroissante," Ann. Ponts. Chaussees **114**, 25–87 (1944).

[6]M. S. Longuet-Higgins, "A Theory of the Origin of Microseisms," Philos. Trans. R. Soc. London Ser. A **243**, 1–35 (1950).

[7]K. Hasselmann, "A Statistical Analysis of the Generation of Microseisms," Rev. Geophys. **1**, 177–210 (1963).

[8]L. M. Brekhovskikh, "Underwater Sound Waves Generated by Surface Waves in the Ocean," Izv. Atmos. Ocean. Phys. **2**, 582–587 (1966) (translated by J. Gollob).

[9]B. Hughes "Estimates of Underwater Sound (and Infra Sound) produced by Nonlinearly Interacting Ocean Waves," J. Acoust. Soc. Am. **60**, 1032–1039 (1976).

[10]S. P. Lloyd, "Underwater Sound from Surface Waves According to the Lighthill–Ribner Theory," J. Acoust. Soc. Am. **69**, 425–435 (1981).

[11]G. L. Tyler, C. C. Teague, R. H. Stewart, A. M. Peterson, W. H. Munk, and J. W. Toy, "Wave Directional Spectra from Synthetic Aperture Observations of Radio Scatter," Deep-Sea Res. **21**, 989–1016 (1974).

[12]K. C. Ewans and A. C. Kibblewhite, "An Examination of Fetch-limited Wave Growth Off the West Coast of New Zealand by a Comparison with the JONSWAP Results" (submitted to J. Phys. Oceanogr., 1989).

[13]K. Hasselmann, T. P. Barnett, E. Bouws, H. Carlson, D. E. Cartwright, K. Enke, J. A. Ewing, H. Gienapp, D. E. Hasselmann, P. Kruseman, A. Mearbug, P. Muller, D. J. Olbers, K. Richter, W. Sell, and H. Walden, "Measurements of Wind-wave Growth and Swell Decay during the Joint North Sea Wave Project (JONSWAP)," Dent. Hydrogr. **2**. Suppl. A8, No. 12 (1973).

[14]K. C. Ewans, "Ocean Waves, Microseisms and their Interrelations," Doctoral dissertation, University of Auckland, New Zealand, 1984.

[15]R. H. Stewart and J. R. Barnum, "Radio Measurements of Oceanic Winds at Long Ranges: An evaluation," Radio Sci. **10**, 853–857 (1975).

[16]M. L. Heron, personal communication (1986).

[17]R. J. Urick, "Seabed Motion as a Source of Ambient Noise Background in the Sea," J. Acoust. Soc. Am. **56**, 1010–1011 (1974).

[18]K. C. Ewans, A. C. Kibblewhite, and P. L. Pearce, "Statistics of the Ocean Wave Field in the Maui Region, 1980–1981," Maui Development Environmental Study, Rep. No. 82–3, University of Auckland, June 1986.

[19]A. C. Kibblewhite and R. N. Denham, "Experiment on Sound Propagation in Shallow Water Under Isovelocity Conditions," J. Acoust. Soc. Am. **40**, 1337–1344 (1966).

[20]L. M. Brekhovskikh, *Waves in Layered Media*, Second ed. translated by R. T. Beyer (Academic, New York, 1980).

[21]D. Rauch, "On The Role Of Bottom Interface Waves In Seismo-Acoustics," a review in *Ocean Seismo-Acoustics*, edited by T. Akal and J. M. Berkson (Plenum, New York, 1986).

[22]T. E. Talpey and R. D. Worley, "Infrasonic Ambient Noise Measurements in Deep Atlantic Water," J. Acoust. Soc. Am. **17**, 621–622 (1984).

[23]H. Schmidt, T. Akal, and W. A. Kuperman, "Low Frequency Wind Generated Ambient Noise In Shallow Water," in *Sea Surface Sound*, edited by B. Kerman (Reidel, Dordrecht, The Netherlands, 1988).